



Title	Performance Analysis of Thermoelectric Modules Consisting of Square Truncated Pyramid Elements Under Constant Heat Flux
Author(s)	Oki, Sae; Natsui, Shungo; Suzuki, Ryosuke O.
Citation	Journal of electronic materials, 47(6), 3288-3297 https://doi.org/10.1007/s11664-017-6055-y
Issue Date	2018-06
Doc URL	http://hdl.handle.net/2115/74513
Rights	This is a post-peer-review, pre-copyedit version of an article published in [Journal of electronic materials]. The final authenticated version is available online at: http://dx.doi.org/10.1007/s11664-017-6055-y
Type	article (author version)
File Information	ICT2017Oki_Ryo20_White-1.pdf



[Instructions for use](#)

1 **Performance Analysis of Thermoelectric Modules**
2 **Consisting of Square Truncated Pyramid Elements**
3 **Under Constant Heat Flux**

4
5 Sae Oki*, Shungo Natsui and Ryosuke O. Suzuki**

6 Faculty of Engineering, Hokkaido University,

7 Kita-13 Jou, Nishi-8 Chome, Kita-Ku, Sapporo, Hokkaido, 060-8628 Japan

8 * s_oki@eng.hokudai.ac.jp, ** Contributing author: rsuzuki@eng.hokudai.ac.jp

9
10 **Abstract**

11 System design of thermoelectric (TE) power generation module is pursued in order
12 to improve the TE performance. Square truncated pyramid shaped P–N pairs of TE
13 elements are connected electronically in series in the open space between two flat
14 insulator boards. The performance of the TE module consisting of 2-paired elements is
15 numerically simulated using commercial software and original TE programs.

16 Assuming that the heat radiating into the hot surface is regulated, i.e., the amount
17 of heat from the hot surface to the cold one is steadily constant, as it happens for solar
18 radiation heating, the performance is significantly improved by changing the shape and
19 the alignment pattern of the elements. When the angle θ between the edge and the base
20 is smaller than 72° , and when the cold surface is kept at a constant temperature, two
21 patterns in particular, amongst the 17 studied, show the largest TE power and efficiency.
22 In comparison to other geometries, the smarter square truncated pyramid shape can
23 provide higher performances using a large cold bath and constant heat transfer by heat
24 radiation.

25

26 **Keywords:**

27 Thermoelectric power generation, constant heat flux, optimum element shape,
28 numerical simulation, square truncated pyramid element

29

30 **1. Introduction**

31 Shapes of thermoelectric (TE) elements ⁽¹⁻⁸⁾ and interesting structures of TE
32 modules (TEM) ⁽⁹⁻¹²⁾ based on heat flow analysis have been recently proposed. The
33 traditional Π -type TE elements are sandwiched between two flat substrates with a heat
34 supplier and a heat receiver, and the thermal heat, introduced from the higher
35 temperature side, transfers to the lower temperature side through TE elements. Some
36 portions of this transferring heat are converted to electricity in the TE material. In
37 addition to the improvement of the performances of the materials, the optimized TE
38 elements design techniques, using three-dimensional simulations along with
39 simultaneous derivative equations, ⁽⁴⁻⁸⁾ predict a larger conversion efficiency for the
40 TEM. Varying its length, a segmented TE element was optimized for the best
41 performance ⁽¹⁾. Other shapes such as cylindrical ^(2,3), parallelogram-like ⁽⁴⁻⁶⁾,
42 trapezoid-like ⁽⁷⁾, truncated square pyramid-like shapes ⁽⁸⁾ have been analyzed. These
43 studies optimized the shapes of TE elements by setting a certain constant temperature
44 difference between the two substrates ⁽¹⁻⁸⁾. The assumption of constant temperature
45 difference is quite easy and suitable for explicit mathematical solutions; however,
46 constant temperature assumptions have a severe practical discrepancy because the
47 majority of TE modules do not work in such an ideal setting; an infinite large thermal
48 bath is required to insure a certain constant fixed temperature, although the assumption
49 of constant temperature difference has been used diffusely since the TE phenomenon
50 was found.

51 On the other hand, a steady heat flow from the hot side may be practically available
52 especially in case of heat radiation. For example, solar heat radiation is in excellent
53 approximation a constant heat source that determines the temperature difference in a TE

54 module and allows a constant heat flow ^(13,14). Depending on the solar energy, the hot
55 side temperature varies allowing TE power generation. Radiation heat from a hot steel
56 slab just after continuous casting is another good example that has been studied lately in
57 Japanese industries ⁽¹⁵⁾.

58 This study examines a design suitable for TE power generation utilizing heat
59 radiation, where the conventional two flat substrates are taken as the basic structure of
60 the TEM. The flat TE panel is commonly used to catch and convert the radiation heat,
61 and a performance enhancement is expected with the introduction of a TE design. The
62 TE analysis presented here is based on a mathematical approach.

63 Our previous work proposed the square truncated pyramidal shape (Fig.1) as a
64 possible geometry for TE elements ⁽⁸⁾, and a slightly slant structure gave both better
65 performance and better efficiency than the conventional Π -type TEM. This shape can
66 suppress the heat transfer from the hot side to the colder side, for instance, when the
67 smaller square surface of a TE element faces the hot surface (Fig. 2). Thanks to the
68 small cross-sectional area of the TE element near the hot side, the heat penetrating into
69 the TE elements may be cut off, and the hot side can be kept at higher temperature.

70 The purpose of this work is to optimize the shape of TE elements theoretically by
71 taking into account that maximum TE power can be obtained with square truncated
72 pyramids while in conditions of constant heat flux. As shown in Fig. 1, the TE
73 performances are measured as a function of the angle between a base and an edge, θ .
74 This shape has four side faces, which may be subject to environmental effects due to the
75 other surrounding elements (such as mutual radiation). In some cases, radiation among
76 TE elements cannot be neglected, and this interaction may contribute constructively to
77 the overall TE output performance. Therefore, 2 pairs of TE elements will be taken as

78 fundamental building block for the analysis of TEM design (Fig. 3).

79 Our previous analysis using parallelepiped⁽⁴⁻⁶⁾ and square truncated pyramids⁽⁸⁾
80 assumed that the temperatures on both the hot and cold surfaces are constant. The
81 performance was maximized at an angle, θ , close to 85 degrees by changing the element
82 shape. The alignment pattern of the elements in the TEM also affected performance and
83 efficiency^(8,9,12). This work is based on the mathematical procedure developed and used
84 in previous works^(16,17), but the requisite for external environment is adjusted for
85 radiation heating.

86

87 **2. Model description and calculation conditions**

88 The length of the basal edge of the cubic TE element is set constant and equal to 1
89 mm. In order to be able to compare the results with those of the previous work⁽⁸⁾, the
90 total volumes of a p- and n-type TE element is set to be 1 mm^3 , as shown in Fig. 4. This
91 assumption is conceived to find a better performance using the same amount of TE
92 material. The angle between the base and the edge, θ , is variable, and the height of the
93 element, h , depends from θ . h becomes bigger as θ is reduced. The angular dependency
94 of h can be fitted with a parabolic approximation. The other variables of the TE element,
95 such as b and c (in Fig. 4), are a function of a and θ , when V is kept constant.

96 Four TE elements are electrically connected in series by thin electrodes, forming a
97 TEM with two flat insulating plates and 5 electrodes, as shown in Fig. 3. θ is varied in
98 the range from 72° to 90° . For $\theta = 90^\circ$, this module is equal to the conventional Π -type
99 module with cubic TE elements. The ratio of cross-sectional area for p- and n-type TE
100 elements has usually been optimized in previous studies by considering the material
101 homogeneous^(1-6, 12, 16, 17), but here the same dimensional size was applied to two kinds

102 of TE element, in order to extract the other factors.

103 In the simulation, three-dimensional heat conduction through solid materials,
104 temperature dependencies of the properties of the materials and the black body heat
105 radiation in vacuum are considered. $\text{Bi}_x\text{Sb}_{2-x}\text{Te}_3$ ⁽⁸⁾ properties are used to simulate the
106 physical properties of p-type TE materials, and those of the n-type TE materials are
107 taken from $\text{Bi}_2\text{Te}_{3-x}\text{Se}_x$ ⁽⁸⁾. These TE properties are listed in Table I as a function of
108 temperature T ⁽⁸⁾. The properties of electrode and insulator materials are selected as pure
109 copper and pure alumina⁽⁸⁾, respectively. These materials have been commonly used by
110 our group^(2-9,12-14,17) in previous studies. The thickness of the electrodes and the
111 insulators are kept at 0.2 mm in all models. The hot source (500 K) is set over the top
112 surface of the TEM, and a constant heat is supplied onto the top surface to simulate the
113 radiated heat. The cold source (300 K) is set beneath the lower surface of the TEM to
114 keep the cold surface of the insulator at a temperature of 300 K. The environmental
115 temperature of the system is set constant at 300 K.

116 This work also examines the effects of the alignment of TE elements. Since the
117 accepted model consist of 2 pairs of p- and n-type elements, four patterns of alignment
118 can be constructed, as shown in Fig. 5: (1) small square surfaces of the elements
119 connected to the hot surface, (2) small square surfaces of the elements connected to the
120 cold surface, (3) small square surfaces of the n-type elements connected to the hot
121 surface, and (4) small square surfaces of n-type elements connected to the cold surface.
122 In order to analyze these four patterns, a model at $\theta = 90^\circ$ and four models at $\theta = 72^\circ$
123 ($\tan \theta = 3$), 76° ($\tan \theta = 4$), 81° ($\tan \theta = 6$) and 85° ($\tan \theta = 12$) are constructed, and then
124 a total of 17 models are simulated.

125

126 **3. Mathematical equations and procedure**

127 The mathematical fundamentals of TE power generation is here explained
128 briefly ^(2-9,12-14,17). Under TE conditions, the heat conduction equation in consideration
129 of the endothermic and exothermic Peltier effects is given by

$$130 \quad \nabla \cdot (\kappa \nabla T) + |\mathbf{J}|/\sigma - T\mathbf{J} \cdot \nabla S = 0, \quad (1)$$

131 where κ , \mathbf{J} , σ and S are the thermal conductivity, current density, electric conductivity,
132 and Seebeck coefficient, respectively. κ , σ and S are defined as a function of temperature
133 T . The equation of the electric field in consideration of the Seebeck effect is given by

$$134 \quad \nabla \cdot (\sigma \nabla V + S\sigma \nabla T) = 0, \quad (2)$$

135 where V is the electric potential. These two differential equations should be
136 simultaneously solved in three-dimensional space. The maximum power and maximum
137 efficiency are calculated by optimizing the external load of the module. The power P
138 generated by the TEM is calculated using the equation

$$139 \quad P = VI = V^2/R, \quad (3)$$

140 where V , I , and R are voltage, current, and the internal resistance of the TEM,
141 respectively. Both V and R are calculated in the simulation for a given design of the
142 module, and V and I are the sum of the simulated values obtained by integrating over all
143 the meshes defined. The current I is determined in order to obtain the power and the
144 efficiency, and their maxima are obtained by optimizing the external resistance. 15-20
145 kinds of resistance were examined to obtain the optimum current in order to get the
146 maximum power, P . The efficiency η is then calculated using the equation

$$147 \quad \eta = P/Q_{\text{input}}, \quad (4)$$

148 where Q_{input} is the heat input from the hot surface of the TEM. Note that Q_{input} is
149 divided into three parts in our model: TE power, conductive heat transmitted to the cold

150 surface and heat dissipated in the surrounding environment as radiation heat. Here Q_{input}
151 is set 500 mW, in order to avoid melting the materials by overheating.

152 The TEM performance was simulated using the commercial software FLUENT
153 (ANSYS Co. Ltd., version 14.0). This software uses the finite-element method (FEM)
154 and can solve heat transfer through solid materials and thermal fluids including heat
155 radiation. Our original program ^(16,17) was embedded in FLUENT to solve the
156 thermoelectric and electric equations governing the Seebeck effect, Peltier effect, and
157 Joule heat generation simultaneously. The hot surfaces were considered to be heated by
158 radiation from the hot source at 500 K and all the surfaces are cooled by radiation in the
159 environment, which is considered to be at normal temperature. The surface of the cold
160 substrate was assumed to be cooled at constant temperature of 300 K by sufficiently
161 large cold source, such as a cool water circulation system. The external conditions are
162 different with Ref. 8, where the terminal temperatures were fixed.

163 The whole analysis of the performance of the TEM took a few hours to complete
164 and the final solution after enough iterations (about 2500) showed a residual error
165 smaller than 10^{-6} . The convergence became slower and the iteration times larger than
166 those achievable assuming the condition of constant temperature difference ⁽⁸⁾. In the
167 FEM analysis the meshes of the model of the TEM are finely divided to assure
168 sufficient preciseness, while the air surrounding the TEM is divided coarsely. This
169 insures both calculation accuracy and shorter calculation time. In addition, the
170 resistance of the electric contact was not considered in the numerical simulation.

171

172 **4. Simulation of TEM performance**

173 **4.1 Distribution of temperature**

174 Fig. 6(1)-(4) show the temperature distributions on the surfaces for the four different
175 patterns of the TEM. The TE elements are square truncated pyramids of $\theta = 72^\circ$. For
176 comparison, the temperature distribution of the TEM whose elements are cubic ($\theta =$
177 90°) is also shown in Fig. 6(0). Fig. 6 shows that the cold insulator and cold electrodes
178 are cooled off homogeneously regardless of the shape; the surface temperature of cold
179 electrodes is kept at 300 K and it is almost the same as the terminal temperature of the
180 TE elements because the electrode material has high thermal conductivity. It can be
181 clearly seen from the temperature distributions that there is no heat loss caused by heat
182 conduction between the two different materials: this is due to the exclusion of the
183 contact thermal resistance from the calculation. As seen in Fig. 6, the upper substrate is
184 the hottest part in all TEM models, but amongst the 4 patterns shown in the figure the
185 highest temperature is reached by pattern 1.

186 Fig. 7 shows the temperature distribution in the central part of the TE element.
187 P-type elements in pattern 0 ($\theta = 90^\circ$) and pattern 2 ($\theta = 72^\circ$) were taken for analysis.
188 The vertical cross-section at the center of a TE element was cut off from the
189 three-dimensional model, and the contour map of temperature was projected onto the
190 section. The temperature profile in pattern 0 ($\theta = 90^\circ$) is completely homogeneous and
191 symmetric from the top surface to the bottom surface, as seen on the square projection
192 (Fig. 7(a)), while the temperature interval in pattern 2 ($\theta = 72^\circ$) is inhomogeneous and
193 shows a fan shaped irregular increment (Fig. 7(b)).

194 In the case of pattern 0 ($\theta = 90^\circ$), heat flows homogeneously without any stagnant
195 point, as shown in Fig. 7(a). In the case of pattern 2 ($\theta < 90^\circ$), the horizontal
196 cross-sectional area at the hot side is wider than that at the cold side. Therefore, the
197 upper part of the TE element is well heated by radiation, or the heat remains stagnant in

198 the upper part. The highest temperature, located at a corner of the upper surface of the
199 TE element ($\theta = 72^\circ$ at Fig. 7(2)), was 457.1 K. However, the lower part of the TE
200 element is cooled by the cold substrate (300 K) and the electrodes, as shown in Fig. 5. A
201 sharp temperature drop can be seen in Fig. 7(b) at the colder side, because the lower
202 surface area is much smaller than the upper surface area.

203 Fig. 8 shows the temperature distribution on the upper surfaces of the TE element
204 terminal, the surface of which is welded with the top substrate (heat receiver). The
205 p-type element in pattern 0 is again taken for analysis. The temperature profile on the
206 surface of pattern 0 looks homogeneous, although a slight deviation, within 0.2 K, can
207 be found. The right corner of the surface shown in Fig. 8 is located close to the center of
208 the TEM, while the left corner is close to the square edge of the top substrate. The heat
209 homogeneously irradiated onto the top substrate should flow into the TE element, and go
210 to the TE element, the opposite terminal of which is cooled by the cold substrate. All the
211 substrates are designed to have larger sizes than the upper surfaces of the TE elements,
212 as shown in Fig. 4 and 5. Because of the larger amount of heat per unit area of the TE
213 element that is accumulated onto the corners of the substrate, the heat is concentrated to
214 the left edge of Fig. 8. This is why the left corner is about 0.25 K hotter than the other
215 corners. Because the center of the top substrate of the TEM is cooled by 4 TE elements,
216 the right corner in Fig. 8 is slightly cooler than the other corners. This inhomogeneity of
217 temperature profile at the upper surface of TE elements was a common feature of all the
218 patterns.

219 All the edges of the upper square surface of the TE elements are about 0.3 K cooler
220 than the central part, as shown in Fig. 8 where they appear blue. This reflects the
221 cooling effect due to thermal radiation from the side surface of the TE elements. In

222 addition, this behavior was the same for all the patterns. Although the temperature was
223 not homogeneous (within 0.3 K deviation), it may be said that is almost constant in the
224 scale of Fig. 6. The temperature difference (ΔT) between two substrates exceeds 157.1
225 K in pattern 2 (Fig.7 (b)), if the average temperature is taken. When θ decreases to
226 values lower than 90° , the temperature of the upper surface increases and ΔT becomes
227 larger. This effect will be discussed later.

228 Fig. 6 also shows that the largest ΔT between two substrates could be obtained in
229 pattern 1, while the smaller ΔT was obtained in pattern 4. Concerning the temperature
230 difference in a TEM model, it is interesting that the temperature profiles of 4 TE
231 elements at $\theta = 72^\circ$ mainly depends on how the elements are aligned (among the 4
232 possible patterns) in respect to the surfaces, showing different behavior depending
233 whether the smaller or the larger surface touches the hot or the cold substrate. The
234 temperature distributions of p- and n-type TE elements in pattern 3 are similar to those
235 of pattern 4. The temperature distributions of the square truncated pyramids in contact
236 with the hot substrates through the smaller surfaces are similar in patterns 1, 3, and 4, as
237 shown in Fig. 6.

238

239 **4.2 Distribution of potential and current**

240 Fig. 9 and 10 show the electric potential and current density distribution,
241 respectively, in TEM models. For the potential distribution, the part shown in red is at a
242 higher potential and that in blue is at a lower potential. The edges of electrodes and
243 elements that are in contact with air had different values compared to their neighbors,
244 but there was no significant influence on the analysis because this occurred only on the
245 top skin of the surface. The total potential difference between two electrode terminals is

246 a measure of the electromotive force (EMF) gained by a TEM model. Because the
247 lowest potential is set 0 at the inlet terminal of the electrode in the simulation, the
248 highest EMF can be obtained at the outlet terminal in pattern 2 ($\theta = 72^\circ$), and the lowest
249 in pattern 0 ($\theta = 90^\circ$).

250 For the distribution of the current density shown in Fig. 10, the red part has a higher
251 current density while the blue part has a lower current density. The current density
252 varies inside the TE element because of the pyramidal shape and the related internal
253 electric resistance. In particular, the corners on the side of the base of the element have a
254 low current density. The existence of low current density area brings the dull
255 performance because these areas do not contribute to charge transport. This result means
256 that the internal current tends to flow preferentially in the shorter circuit such as the
257 central part of the TE element ⁽⁸⁾. Meng et al. proposed a slant TE element based on this
258 concept ⁽⁴⁻⁶⁾.

259 The highest current density is often marked in the shallow electrodes, as shown in
260 pattern 2 and 4 in Fig. 10. It is noted, however, that the patterning and width of the
261 electrode channels did not affect the performance of the individual models. This
262 happens because the low electric resistivity of electrode material (copper) with
263 sufficient thickness does not affect the total performance of the TEM.

264 Fig. 6 (0), Fig. 9 (0) and Fig. 10 (0) show the temperature distribution, potential
265 distribution and current density distribution, respectively, for pattern 0 ($\theta = 90^\circ$). They
266 show the temperature difference between the substrates ($\Delta T =$ about 65 K), potential
267 difference ($\Delta E = 45.37$ mV) and current ($I = 0.32$ A) between two electrode terminals
268 under constant heat flow (500 mW). They are much smaller than those obtained for
269 fixed temperatures of the substrates for pattern 0 ⁽⁸⁾. For example, the previous study ⁽⁸⁾

270 showed that $\Delta E = 126.2$ mV and $I = 1.06$ A, respectively, at $\Delta T = 200$ K in pattern 0 (θ
271 $= 90^\circ$).

272 It should be noted here that all the data given in Fig. 6, 9 and 10 were obtained after
273 optimizing the external resistance of each TEM model for maximum power, as
274 mentioned below.

275

276 **4.3 Power of TEM**

277 If a TEM is connected to an external resistance, the internal current is affected by
278 the external resistance according to the laws of serial connection in circuit theory.
279 Therefore, power generally varies as a parabolic function of current, and there exists a
280 maximum for the power output. The maximum power and maximum efficiency of a
281 certain TEM model can be obtained for the same conditions of current, i.e., the same
282 external resistance. Because Peltier heat works in addition to Joule heat, the current
283 generated has a non-linearly relationship with the voltage. The internal resistance
284 depends on temperature as a function of the properties of the materials; moreover, the
285 Peltier effect also depends on temperature. In this study, we numerically simulate them
286 both by controlling the external resistance.

287 **Fig. 11** shows an example of the voltage, V , power, P , and efficiency, η , as a
288 function of the current, I , for $\theta = 85^\circ$ in pattern 2. As typical behavior of an electric
289 serial circuit, the power obtainable from the TEM decreases at currents both smaller and
290 larger than the optimal current. A small deviation in P near P_{\max} is due to a small
291 uncertainty in numerical calculation and the non-linear behavior of V as function of I .
292 The latter is due to non-linear temperature dependencies of the properties of the material
293 in TE effects.

294 The evaluated maximum power P_{\max} is summarized as a function of θ in Fig. 12. The
295 largest P_{\max} in this work is obtained at $\theta = 72^\circ$ for all of the alignment patterns of the
296 TE element. It is noted that $\theta = 72^\circ$ is the lowest angle in the studied range. A model
297 with an angle smaller than 72° was not easily constructed in the numerical mesh
298 generation process. Overly thin cells did not give stable and reproducible results during
299 numerical calculation. In this work, the mesh forming policy in the TEM model
300 construction was unified and fair for all the models. It is noted that smaller cells in
301 simulation need a larger computer capacity. The experiments with an angle smaller than
302 72° may overcome this numerical difficulty to obtain the larger P_{\max} .

303 The electric voltage becomes larger when θ is smaller than 90° , as shown in Fig. 9,
304 because the temperature difference ΔT increases. It is clear that, according to Eq. (3),
305 the obtainable P_{\max} becomes larger when the electromotive force increases. The trend of
306 an increasing P_{\max} with a reducing θ , therefore, is a common feature found in all the
307 studied alignment patterns of the TE elements (Fig. 12).

308 The maximum power obtainable with the assumption of constant temperature
309 difference⁽⁸⁾ was compared with this work in Fig. 12. P_{\max} for constant ΔT decreased as
310 θ decreased. This trend was opposite to that found in this work (constant heat flux). For
311 example, 1.869 W was lost as penetration heat in the pattern 0, when $\Delta T = 200$ K and θ
312 $= 90^\circ$, and this heat decreased as θ decreased. However, in this work, we assume a
313 constant heat flux of only 500 mW for all the models, and we find that the temperature
314 difference increases due to the effect of the TE element shape as θ decreases.

315

316 **4.4 Radiation from TEM**

317 Fig. 12 shows that the modification of the shape of an element has a strong influence

318 on P_{\max} as a function of θ , while the patterns of the element alignment have a relatively
319 smaller influence on P_{\max} than the contribution of θ . This sensitivity to the alignment
320 may come both from the contributions of temperature dependencies of the properties of
321 various materials and from heat exchange among the other TE elements due to heat
322 radiation. Here the contribution from the radiation is analyzed.

323 Fig. 13 shows the numerical summation of heat, Q , radiated from all the trapezoidal
324 side surfaces of the TE elements. The ratio of Q/Q_0 varies from 1% to 7% depending on
325 θ , where Q_0 is the constant heat flux (500 mW). Because the temperature of a TE
326 element surface is hotter (Fig. 6) as θ decreases, it is natural that the amount of heat
327 radiation becomes larger. It is additionally noted that the side surface area, S , is larger
328 (Fig. 4) as θ decreases. For example, S at $\theta = 72^\circ$ is 18% larger than S at $\theta = 90^\circ$.
329 Radiant heat from a wider S is larger, as shown Fig. 13. Therefore, the increment of side
330 surface area of the TE elements and the heating of these surfaces are two major reasons
331 why we found an increased amount of radiation heat for smaller θ .

332 At a certain θ , the heat radiation in pattern 1 is smaller than in pattern 2. The amounts
333 of radiation heat in pattern 3 and pattern 4 are almost identical within numerical error,
334 as seen in Fig. 13. This evidences a good symmetry of alignment of the TE elements in
335 these two patterns. Generally, the radiated heat is not converted into electricity, and it
336 lowers the TE performance. Therefore, the smaller P_{\max} of pattern 1 compared to that of
337 pattern 2 (Fig. 12) is partially due to the radiation loss of penetrating heat, although the
338 amount of radiation heat is less than 7% that of penetration heat, Q_{input} . If we assume
339 that the radiation plays some role in P_{\max} , the difference in P_{\max} between patterns 3 and
340 4 is due to the characteristics of the materials such as electric and thermal
341 conductivities.

342 In short, the contribution of radiation heat to TE performance is secondary compared
343 with that of shape. Moreover, the amount of radiation heat depends on the shape
344 because of the surface area and temperature profile. The effects of different TE elements
345 alignments to radiation are well limited as shown in Fig. 13. This short summary is
346 valid in the mild temperature range studied in this work. When the TEM is heated to a
347 temperature range where radiation becomes dominant, its contribution cannot be longer
348 neglected.

349

350 **4.5 Efficiency of TEM**

351 Since the efficiency, η , is defined as in eq. (4), η is proportional to P , and the
352 optimum current that achieves P_{\max} is identical to that that achieves also η_{\max} , as shown
353 in Fig. 11. The angular dependence of the maximum efficiency η_{\max} was, however,
354 different from that found in our previous work⁽⁸⁾, as shown in Fig. 14. The largest η_{\max}
355 at constant heat flux conditions was obtained when $\theta = 72^\circ$ in pattern 2. In this
356 alignment, all the small square surfaces of the element terminals are connected to the
357 cold surface. Because the high temperature zone is extended to the cooler part as shown
358 in Fig. 6 (2), a large amount of heat is lost as radiation from the side surfaces as shown
359 in Fig. 13. Even so, a high temperature difference and the corresponding high potential
360 difference increase the output power, and the highest efficiency in TE power generation
361 is obtained in pattern 2.

362 Fig. 14 also shows that the η_{\max} at constant temperature difference were larger than
363 those at constant heat flux conditions. The former is not so seriously dependent on angle,
364 and the latter exceeds the former especially at the smaller angles such as $\theta = 72^\circ$.

365 The performance of the TEM will possibly be further improved by changing the

366 shape of the TE element in consideration of the best matching between the temperature
367 distribution of the materials and the properties of the materials in the given temperature
368 range.

369

370 **5. Conclusion**

371 The combination of square truncated pyramid elements and flat plate shape was
372 examined using numerical simulation. Taking into account the temperature dependence
373 of the materials, the possibility of constructing a suitably shaped TEMs optimized for
374 high efficiency was proposed. Under the constraint of constant heat flow through the TE
375 module, the output of the TEM and the yield of input energy were numerically
376 evaluated by solving the related differential equations. The angle θ between the edges of
377 the square truncated pyramid was taken as an analytical parameter to describe the TE
378 shape, and the smallest θ gave the greatest output and the higher yield. This happens
379 because the suppression of heat transfer in the TE elements due to small cross-sectional
380 area can give the larger temperature difference. This trend was opposite in the case of
381 constant temperature assumption as reported in our previous study.

382 Two patterns, 2 and 4, showed the best performance based on good heat extraction
383 to the lower positions and on nice matching with the temperature dependency of the
384 properties of the materials, although the radiation heat from the side surface increases.
385 The shapes, as the square truncated pyramid, and alignments were proposed for TE
386 elements.

387

388 **Acknowledgments**

389 The program used here was originally coded by Dr. Min Chen at Aalborg University,

390 Denmark, and revised by Mr. Takeyuki Fujisaka at Hokkaido University (now at
391 Nippon Steel & Sumitomo Metal Co., Japan), and was modified specifically for this
392 paper. This work was financially supported in part by Grant-in-Aid for Challenging
393 Exploratory Research (Japan Society for the Promotion of Science, No. 26630490), and
394 The Thermal & Electric Energy Technology Foundation.

395

396 **References**

- 397 [1] J. D'Angelo, E. D. Case, N. Matchanov, C. Wu, T. P. Hogan, J. Barnard, C. Cauchy,
398 T. Hendricks, and M. G. Kanatzidis, *J. Electr. Mater.*, **40** (10), 2051-2062 (2011).
- 399 [2] R. O. Suzuki and D. Tanaka, *J. Power Sources*, **124** (1) 293-298 (2003).
- 400 [3] T. Kyono, R. O. Suzuki and K. Ono, *IEEE Transactions on Energy Conversion*, **18**
401 (2) 330-334 (2003).
- 402 [4] X.-N. Meng, T. Fujisaka, K. O. Ito and R. O. Suzuki, *Mater. Trans.*, **55** (8),
403 1219-1225 (2014).
- 404 [5] X.-N. Meng and R. O. Suzuki, *J. Electr. Mater.*, **44** (6), 1469-1476 (2015).
- 405 [6] X.-N. Meng and R. O. Suzuki, *Mater. Trans.*, **56** (7) 1092-1095 (2015).
- 406 [7] S. Oki, K.O. Ito, S. Natsui and R.O. Suzuki, *J. Electr. Mater.*, **45**, (3), 1358-1364
407 (2016).
- 408 [8] S. Oki and R.O. Suzuki, *J. Electr. Mater.*, **46** (5) (2017) 2691-2696.
- 409 [9] R. O. Suzuki and D. Tanaka, *J. Power Sources*, **132** (1-2) 266-274 (2004).
- 410 [10] T. Kanno, A. Sasaki, K. Takahashi, A. Omote, H. Adachi and Y. Yamada, *Appl.*
411 *Phys. Lett.*, **101**, 011906 (2012).
- 412 [11] D.T. Crane, J. W. LaGrandeur, F. Harris, L. E. Bell, *J. Electr. Mater.*, **38** (7) (2009)
413 1375-1381.
- 414 [12] R. O. Suzuki and D. Tanaka, *J. Power Sources*, **122** (2) 201-209 (2003).
- 415 [13] R. O. Suzuki, K. O. Ito and S. Oki, *J. Electr. Mater.*, **45** (3) 1827-1835 (2016).
- 416 [14] R. O. Suzuki, T. Fujisaka, K. O. Ito, X. Meng and H.-T. Sui, *J. Electr. Mater.*, **44**
417 (1) (2015) 348-355.
- 418 [15] T. Kuroki, K. Kabeya, K. Makino, T. Kajihara, H. Kaibe, H. Hachiuma, H.
419 Matsuno, A. Fujibayashi, *J. Electr. Mater.*, **43** (6) (2014) 2405-2410.

- 420 [16] M. Chen, L.A. Rosendahl, and T. Condra, *Inter. J. Heat Mass Transf.*, **54**, 345-355
421 (2011).
- 422 [17] T. Fujisaka, H. Sui, and R. O. Suzuki, *J. Electr. Mater.*, **42**, (7), 1688-1696 (2013).
423

424 **Table caption**

425 Table I Thermophysical properties of two TE materials⁽⁸⁾

426

427 **Figure captions**

428 Fig. 1 Thermoelectric element with square truncated pyramid shape.

429 Fig. 2 Concept of a module with TE elements of square truncated pyramid shape.

430 Fig. 3 Dimensions of TE elements and the other parts (in unit of mm)⁽⁸⁾.

431 Fig. 4 Angular dependency of dimensions of the studied element. V and S are volume
432 (set constant as 1 mm^3) and surface area of an element, respectively.

433 Fig. 5 Four patterns of alignments (1)-(4) at $\theta = 72^\circ$, and an alignment (0) at $\theta = 90^\circ$
434 for reference⁽⁸⁾.

435 Fig. 6 Temperature distribution in the TEM. (1)-(4) Four patterns of alignments at $\theta =$
436 72 degree. (0) the distribution at $\theta = 90^\circ$ for reference.

437 Fig. 7 Contour map of temperature at the central cross-section of a TE element;
438 (a) $\theta = 90^\circ$ (pattern 0) and (b) $\theta = 72^\circ$ (pattern 2).

439 Fig. 8 Contour map of temperature at the top surface of the TE element located at
440 right-end corner in Fig. 5 (0); $\theta = 90^\circ$ (pattern 0).

441 Fig. 9 Electric potential distribution in the TEM. (1)-(4) Four patterns of alignments at
442 $\theta = 72^\circ$. (0) the distribution at $\theta = 90^\circ$ for reference.

443 Fig. 10 Distribution of current density in the TEM. (1)-(4) Four patterns of alignments
444 at $\theta = 72^\circ$. (0) the distribution at $\theta = 90^\circ$ for reference.

445 Fig. 11 Relationship among current, voltage, power and efficiency in pattern 2 at $\theta =$
446 85° .

447 Fig. 12 Maximum power generated by TEM as a function of angle. Broken line:
448 maximum power in case surface temperature is fixed ($\Delta T=200\text{ K}^{(8)}$).
449 Fig.13 Radiated heat from TE elements surface.
450 Fig. 14 Maximum efficiency generated by TEM as a function of angle.
451

452

Table I Thermophysical properties of two TE materials ⁽⁸⁾

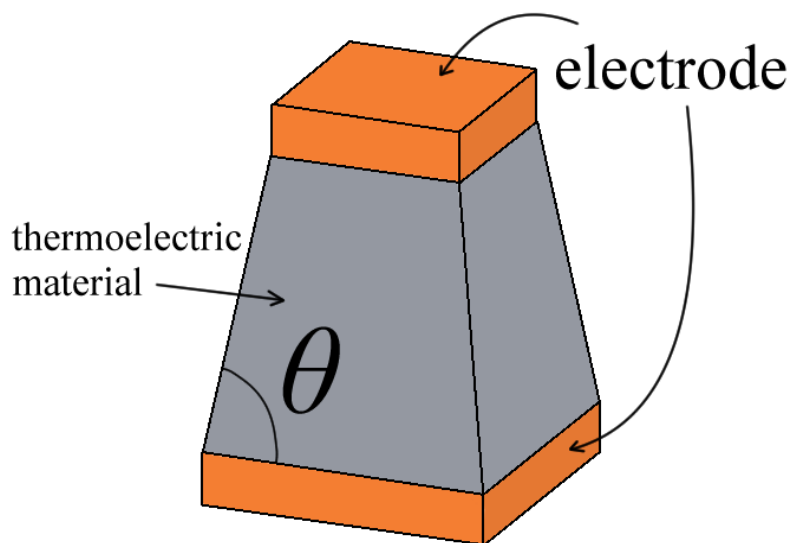
453

454

Material:p-type Bi _x Sb _{2-x} Te ₃	Temperature, T/K
Electric conductivity, $\sigma \times 10^2 / \text{S cm}^{-1}$	
$\sigma = -473.1 + 0.86507T - e^{16.637 - 1.6942 \ln(T)}$	300-560
Seebeck coefficient, $S / \mu\text{V K}^{-1}$	
$S = -188.2 + 2.2411T - 3.0075 \times 10^{-3}T^2 + 2.4914 \times 10^{-7}T^3$	
Thermal conductivity, $\kappa / \text{W m}^{-1} \text{K}^{-1}$	250-560
$\kappa = -1.8067 + 5.7529 \times 10^{-3}T - 64.639/T + 1.3395 \times 10^5/T^2$	
Material:n-type Bi ₂ Te _{3-x} Se _x	Temperature, T/K
Electric conductivity, $\sigma \times 10^2 / \text{S cm}^{-1}$	
$\sigma = -2139.4 + 2.5778T + e^{12.765 - 0.89092 \ln(T)}$	300-560
Seebeck coefficient, $S / \mu\text{V K}^{-1}$	
$S = 443.49 - 4.5121T + 9.4424 \times 10^{-3}T^2 - 5.8362 \times 10^{-6}T^3$	
Thermal conductivity, $\kappa / \text{W m}^{-1} \text{K}^{-1}$	250-560
$\kappa = -4.6205 + 833.7/T + 23536/T^2$	

455

457



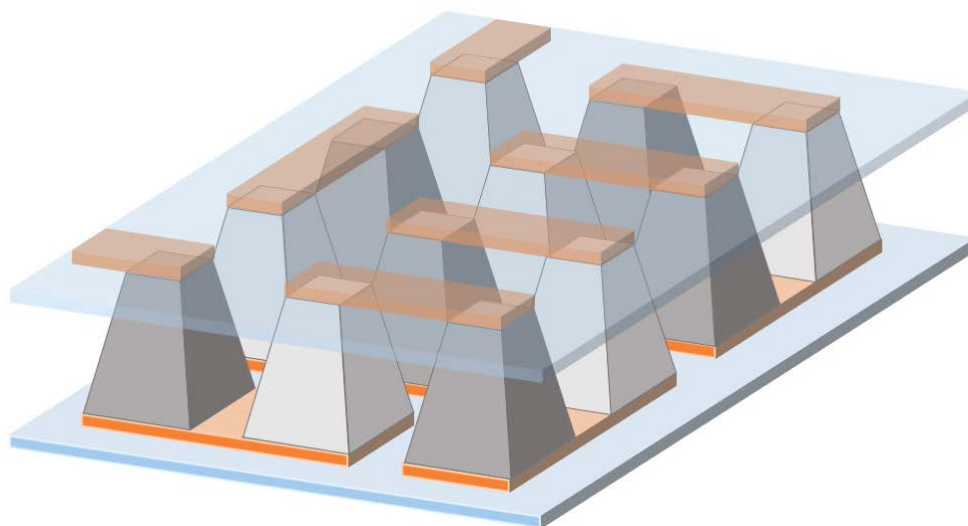
458

459

460

Fig. 1 Thermoelectric element with square truncated pyramid shape.

461



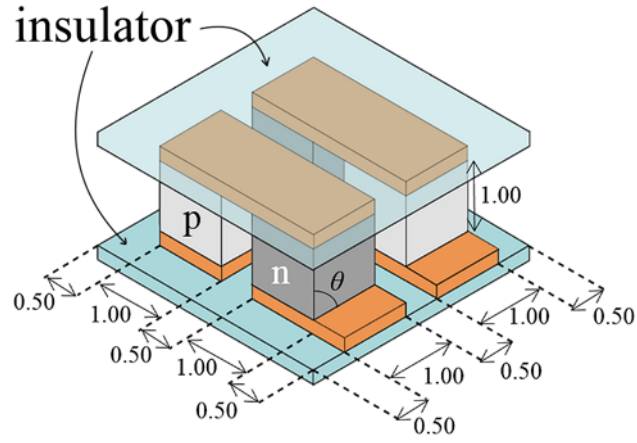
462

463

464

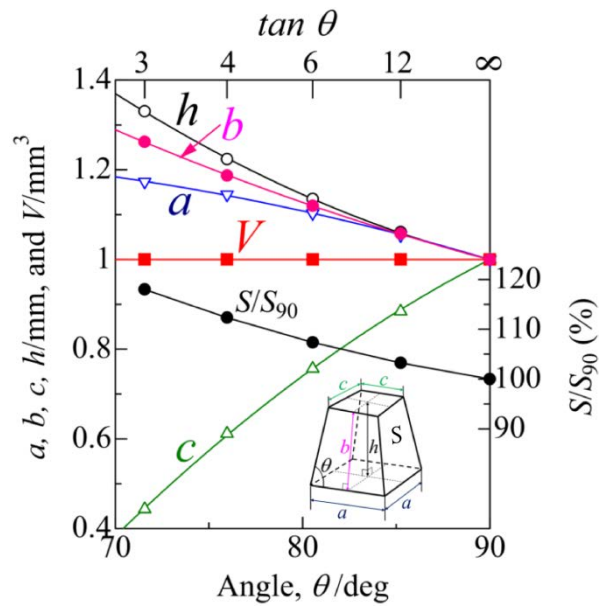
Fig. 2 Concept of a module with TE elements of square truncated pyramid shape.

465



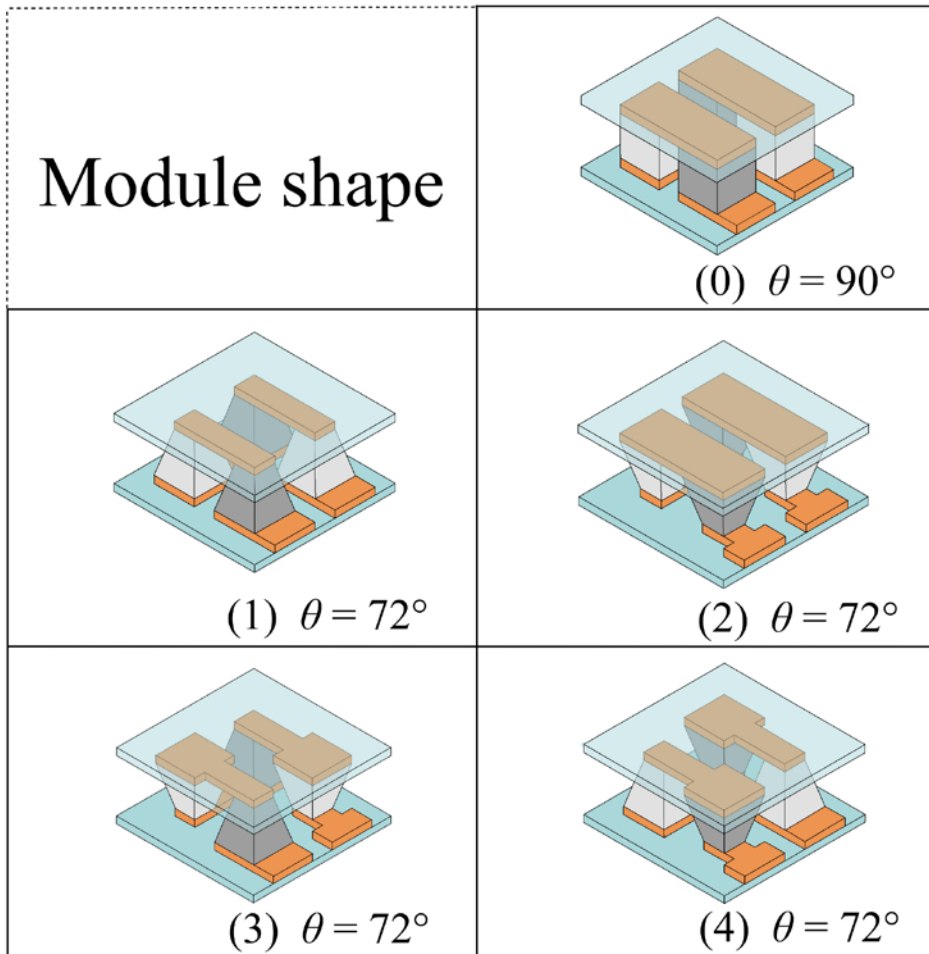
466
467
468

Fig. 3 Dimensions of TE elements and the other parts (in unit of mm)⁽⁸⁾.



469
470
471
472

Fig. 4 Angular dependency of dimensions of the studied element. V and S are volume (set constant as 1 mm³) and surface area of an element, respectively.



473

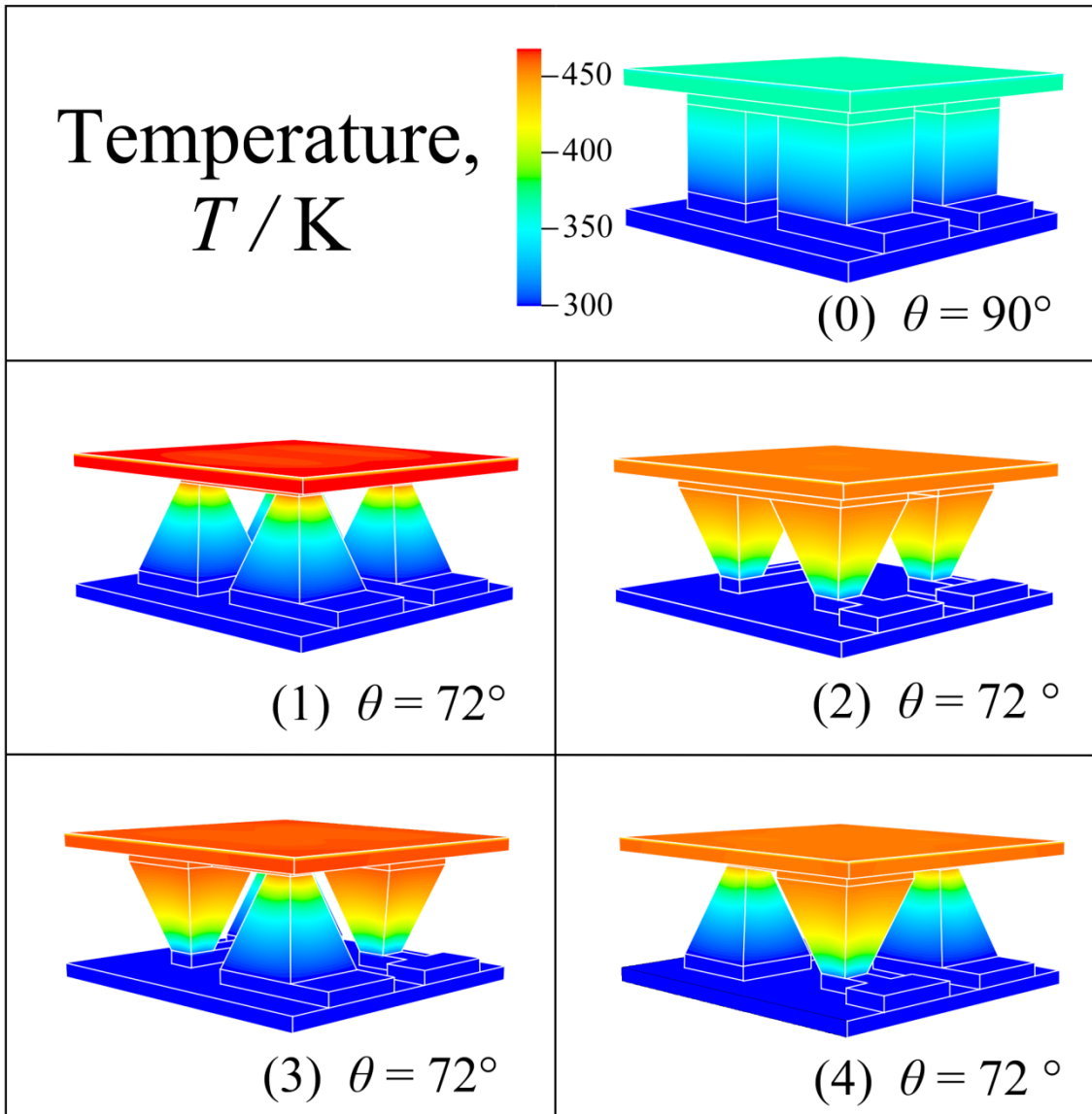
474

Fig. 5 Four patterns of alignments (1)-(4) at $\theta = 72^\circ$, and

475

an alignment (0) at $\theta = 90^\circ$ for reference ⁽⁸⁾.

476



477

478

479

480

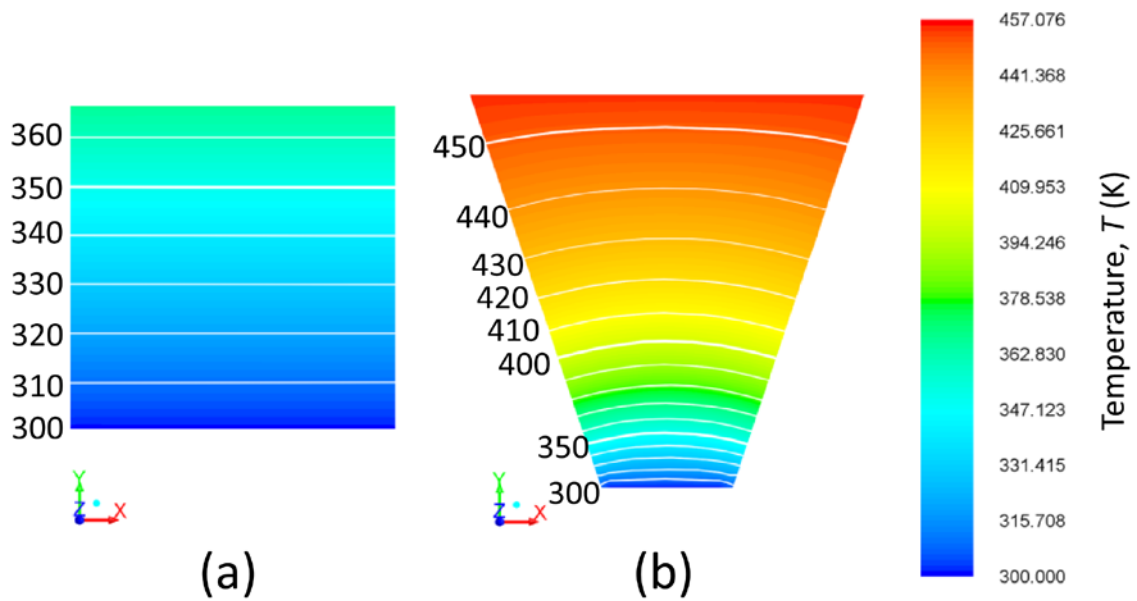
481

482

Fig. 6 Temperature distribution in the TEM.

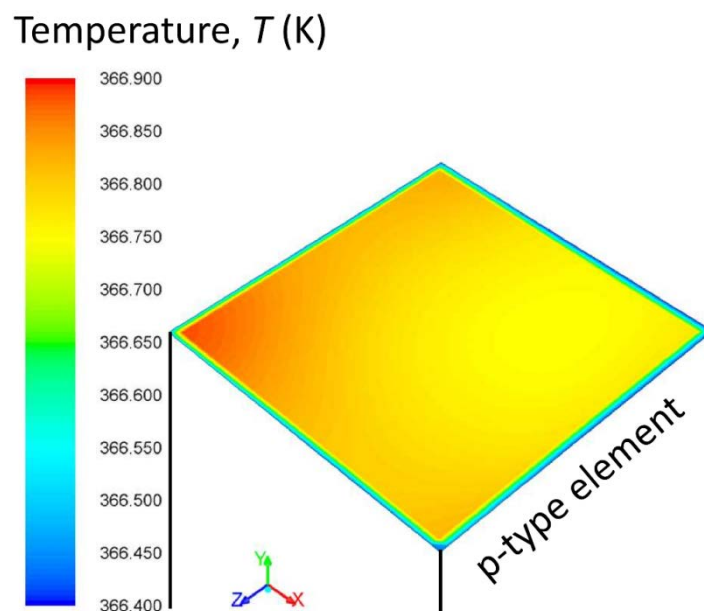
(1)-(4) Four patterns of alignments at $\theta = 72^\circ$.

(0) the distribution at $\theta = 90^\circ$ for reference.



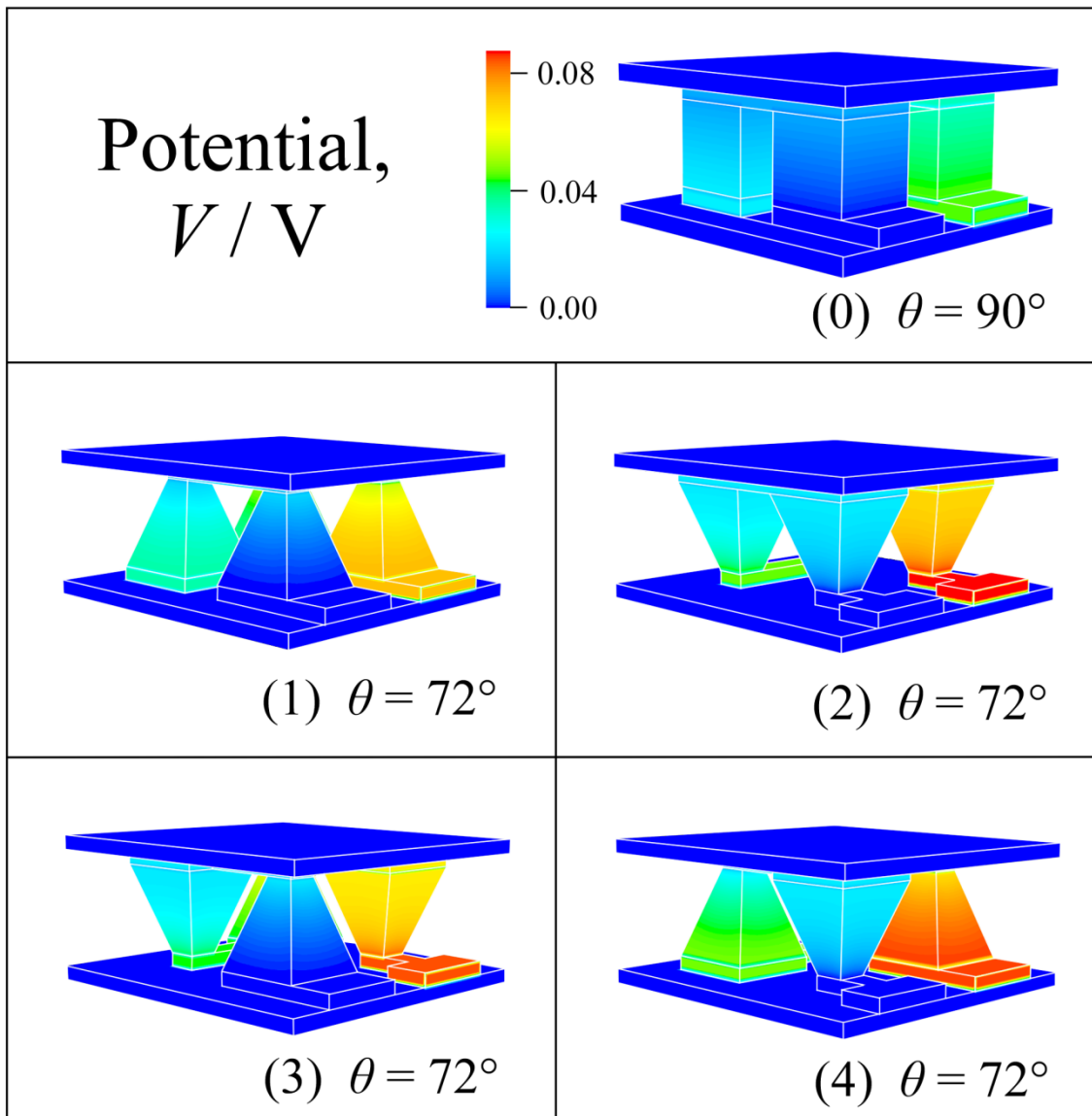
483
484
485
486
487

Fig. 7 Contour map of temperature at the central cross-section of a TE element;
(a) $\theta = 90^\circ$ (pattern 0) and (b) $\theta = 72^\circ$ (pattern 2).



488
489
490
491
492

Fig. 8 Contour map of temperature at the top surface of the TE element located at left-end corner in Fig. 5 (0); $\theta = 90^\circ$ (pattern 0).



493

494

495

496

Fig. 9 Electric potential distribution in the TEM.

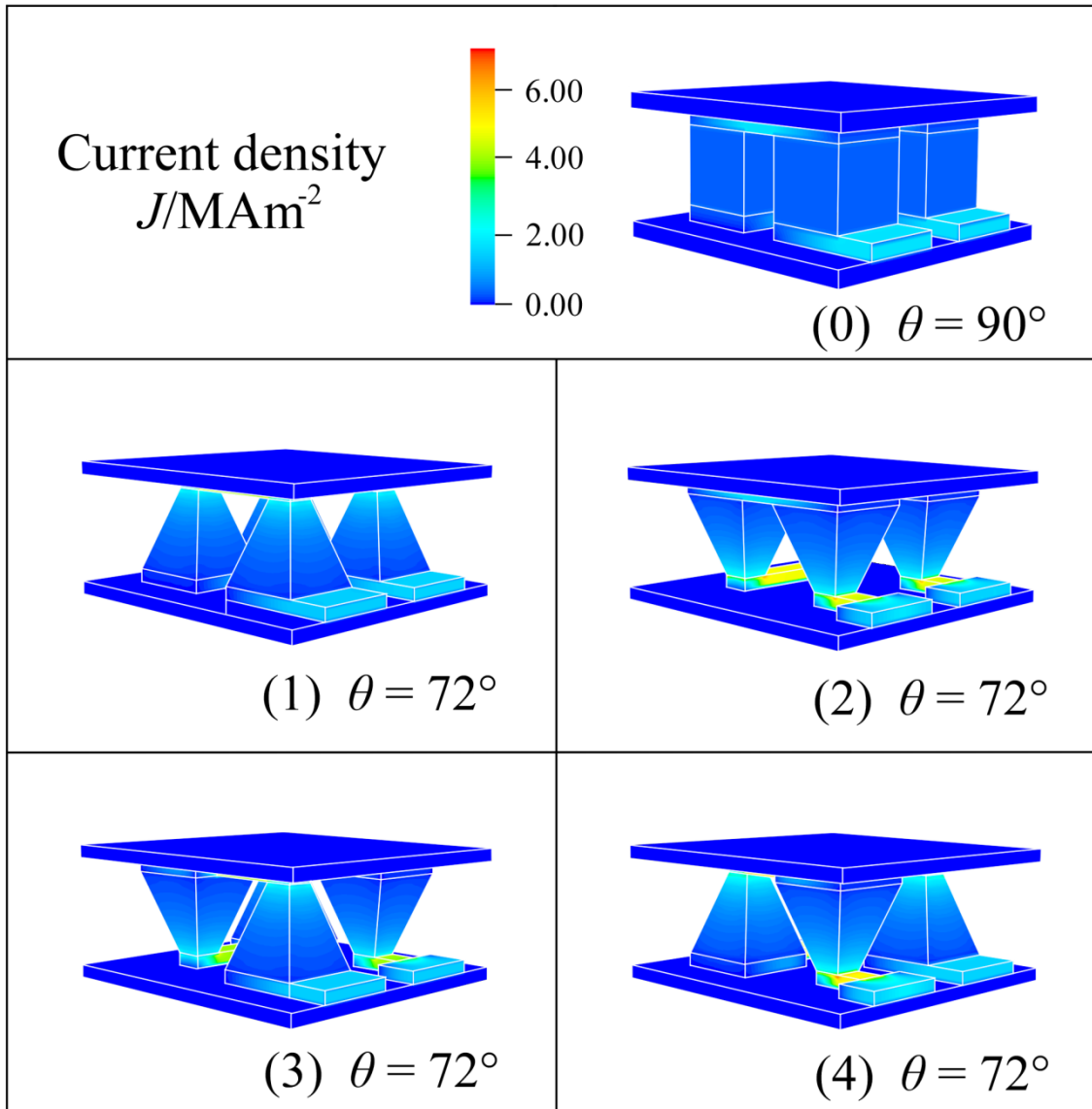
497

(1)-(4) Four patterns of alignments at $\theta = 72^\circ$.

498

(0) the distribution at $\theta = 90^\circ$ for reference.

499



500

501

502

503

Fig. 10 Distribution of current density in the TEM.

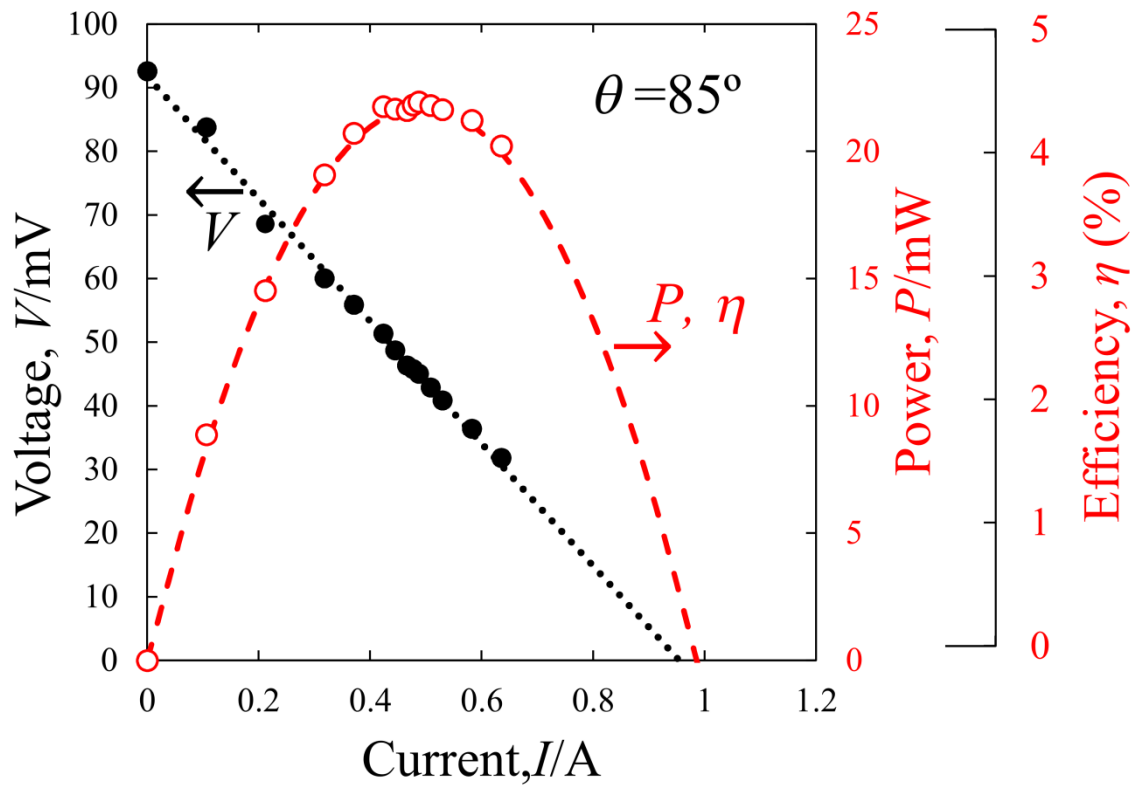
504

(1)-(4) Four patterns of alignments at $\theta = 72^\circ$.

505

(0) the distribution at $\theta = 90^\circ$ for reference.

506

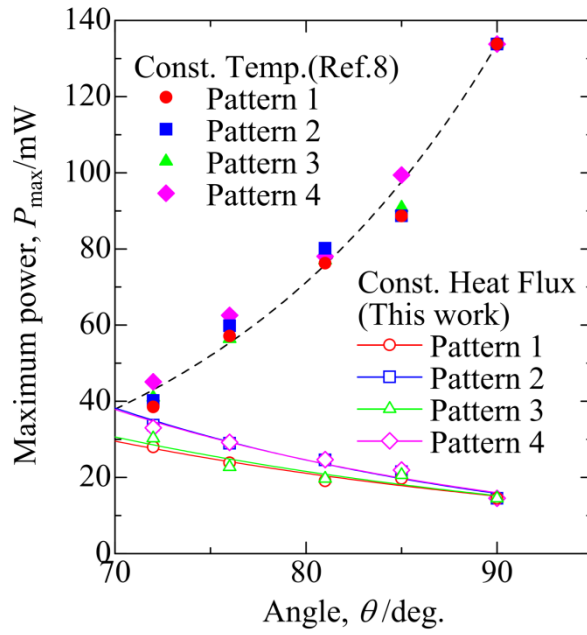


507

508

509 Fig. 11 Relationship among current, voltage, power and efficiency in pattern 2 at $\theta =$
 510 85° .

511



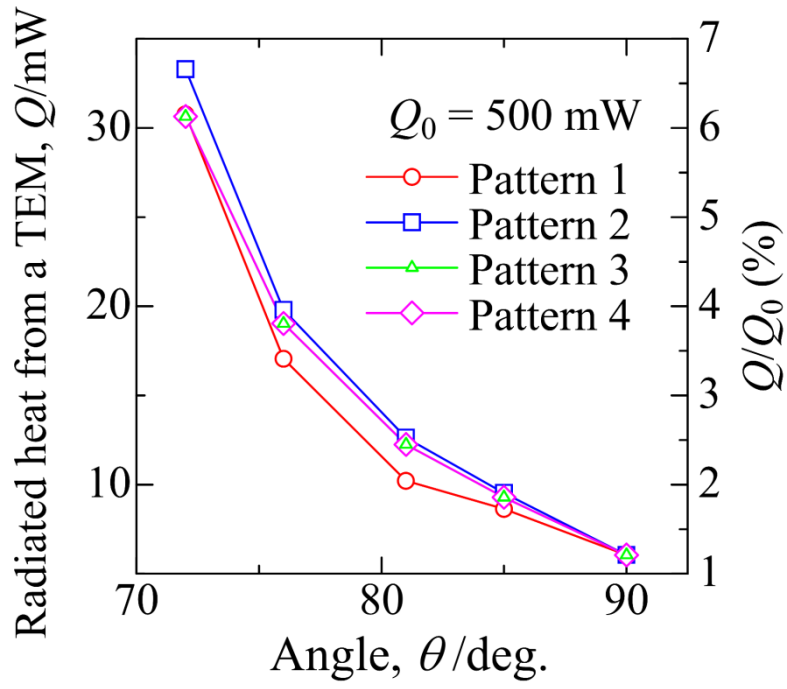
512

513

514 Fig. 12 Maximum power generated by TEM as a function of angle. Broken line:

515 maximum power in case surface temperature is fixed ($\Delta T=200$ K⁽⁸⁾).

516



517

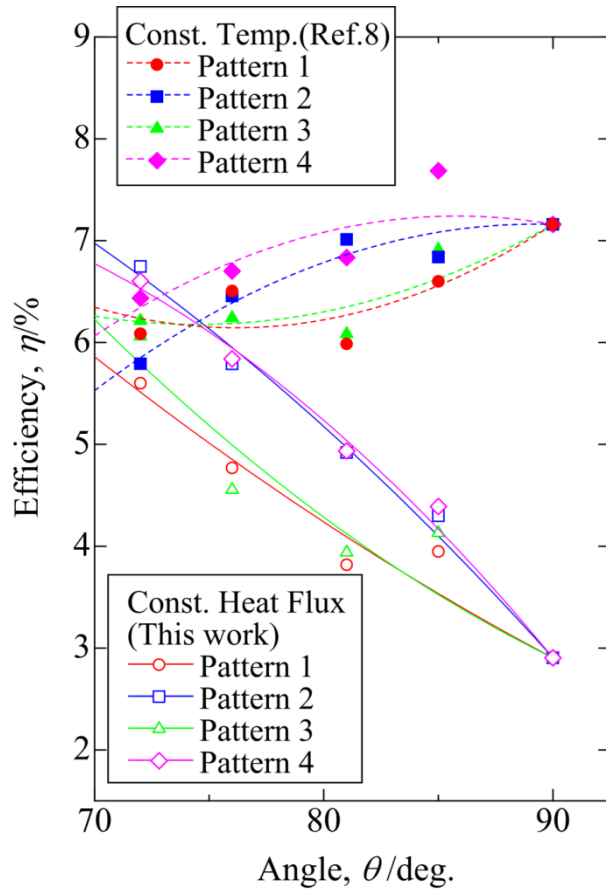
518

519

520

Fig.13 Radiated heat from TE elements surface.

521



522

523

524

Fig. 14 Maximum efficiency generated by TEM as a function of angle.

525